Case Studies in Thermal Engineering 36 (2022) 102173

Contents lists available at ScienceDirect

Case Studies in Thermal Engineering

journal homepage: www.elsevier.com/locate/csite

Latent heat induced deformation of PCB substrate: Measurement and simulation

Denis Froš *, Petr Veselý, Jan Zemen, Karel Dušek

Department of Electrotechnology, Faculty of Electrical Engineering, Czech Technical University in Prague, Prague, Czech Republic

GRAPHICAL ABSTRACT

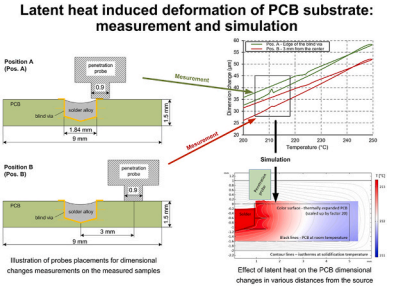

ARTICLE INFO

Keywords:
Soldering
PCB substrate
Thermal expansion
Latent heat
FEM analysis

ABSTRACT

The work evaluates the impact of latent heat (LH) absorbed or released by a solder alloy during melting or solidification, respectively, on changes of dimensions of materials surrounding of the solder alloy. Our sample comprises a small printed circuit board (PCB) with a blind via filled with lead-free alloy SAC305. Differential scanning calorimetry (DSC) was employed to obtain the amount of LH per mass and a thermomechanical analyzer was used to measure the thermally induced deformation. A plateau during melting and a peak during solidification were detected during the course of dimension change. The peak height reached 1.6 μm in the place of the heat source and 0.3 μm in the distance of 3 mm from the source. The data measured during solidification was compared to a numerical model based on the finite element method. An excellent quantitative agreement was observed which confirms that the transient expansion of PCB during cooling can be explained by the release of LH from the solder alloy during solidification. Our results have important implications for the design of PCB assemblies where the contribution of recalescence to thermal stress can lead to solder joint failure.

* Corresponding author.
E-mail address: frosdeni@fel.cvut.cz (D. Froš).

https://doi.org/10.1016/j.csite.2022.102173
Received 13 April 2022; Received in revised form 22 May 2022; Accepted 3 June 2022
Available online 8 June 2022

1. Introduction

Reflow soldering is a process that requires high temperature to produce the electrical connection in the form of a solder joint. Assembled printed circuit board (PCB) must go through this thermal treatment for the purpose of solder paste reflow. The thermal procedure always initiates thermomechanical stress put on the assembly. In conjunction with current lead-free alloys, the assembly is exposed to the maximal temperature around 250 °C. To ensure the formation of a reliable solder joint and to avoid the failure of some PCB parts during soldering, it is desirable to adjust reflow procedures correctly and choose suitable materials [1]. Despite fulfilling the process requirements, a mismatch in coefficients of thermal expansion (CTE) is responsible for the arising thermomechanical stress that has an adverse impact on certain parts of PCB. Additionally, the influence of the thermomechanical stress is exacerbated by the uneven distribution of thermal fields on the PCB. Concurrently, the inhomogeneous field is accompanied by a shrinkage of the board. Moreover, internal residual stress may occur in some materials as a result of their previous manufacturing steps, like in the case of the PCB [2]. This stress can be released during the first reflow soldering cycle and contributes to the overall stress accumulated in certain areas with an increased probability of failure. An example of a high-risk area susceptible to dynamic and excessive dimension changes are the surroundings of plated through holes (PTH) or places with a higher density of soldering pads located very close to each other. The origin and consequences of the stated phenomena are enhanced by the complex design of PCBs. Multi-layered boards adopting a large number of small plated holes (microvias) and high-density interconnection are typical parts of today's electronic devices.

Fabrication of the conventional PCB substrate involves two basic materials such as glass cloth and resin. In terms of thermal properties, a resin used for the reinforcement impregnating is classified by glass transition temperature (Tg), delamination temperature and decomposition temperature [3]. Tg value determines the rapid change of the CTE in the Z-axis. Other laminate properties (e.g., Young's modulus, heat capacity) and structure become different too. Considerable transformation of the CTE certainly occurs during the soldering process. To achieve better thermal stability and thereby higher resilience and the possibility of multiple reflows, curing agents making higher cross-linking system and other additives are added to the original resin compound. Not fully cured resin may affect the thermomechanical behavior of the board. Rudajevová and Dušek [4] studied residual strain in the presence of Cu plated holes and detected its release during the first thermal cycle. Material vertical expansion can result in cracking of PTH and separation of the microvia base and the soldering pad [5,6]. Currently, experimental methods are being substituted by finite element modeling that is utilized to estimate PTH and vias reliability [7,8]. The relationship between plated hole reliability and Tg value was investigated by Reutzel [9]. The study proves the impact of laminate Tg on PTH failure. Holes with smaller diameters were detected to be more prone to cracking.

Considering the slimness, complexity, and miniaturization of the PCBs, generation of board warpage is facilitated upon heating. Shrinkage is supported by the mismatch of CTE. PCBs shapes and heat transfer coefficients that vary based on reflow types (convection, vapor phase, infrared etc.) play an important role in the thermomechanical behavior of the assembly, too [10,11]. This issue concerning different physical properties within the whole assembly as well as processing conditions may result in establishing an electrically non-conductive joint when components like BGA (Ball Grid Array) or CSP (Chip Scale Package) are assembled. A typical defect is known as head-in-pillow [12]. Bušek et al. [13] suggest that warpage promotes detachment of already created joint. Among problems connected with warpage effect phenomena called pad cratering must be included [14]. Due to board shrinkage, forces impact not only solder joints but also the soldering pads. If the force exceeds the endurable limit, the pad is peeled off or torn from the substrate. These two listed concerns happen at the moment when the temperature is further below the melting point but the board or the component still tends to warp. Warpage effect is reduced by using a sandwich structure that was studied by Pietrikova et al. [15]. This structure provides higher flexural stiffness and strength which decreases the twisting tendency of the assembly.

Current alloys are largely made of tin with a small addition of noble metal such as silver or copper. Distinctions in metal composition (particularly lead elimination) lead to changes in thermal properties of the solder alloys and consequently solder joints [16]. Different thermomechanical conditions are caused by different heat capacities, thermal conductivity, and CTEs of the metal elements and compounds forming the joint. Regarding the parameters mentioned above, thermal conditions must be appropriately set for a specified alloy during the soldering process. Moreover, solder alloys absorb and release latent heat during the reflow soldering. It was clarified by Dušek et al. [17] that latent heat influences the shape of the temperature profile during heating and cooling. Morando et al. [18] confirmed the fluidity length of the solder alloys to be dependent on latent heat, too. In the case of the area with a high density of joints to be soldered, the solidification of solder joint occurring in the neighborhood of surrounded solder joints may be delayed due to the release of latent heat during solidification [19]. Also, Dušek and Rudajevová [20] revealed that latent heat contributes to the risk of tearing the pad from the substrate because the latent heat of solidification locally softens the resin beneath the soldering pad while farther vicinity is already in the rigid state.

This study deals with the investigation of the consequences caused by latent heat release. We focused on the secondary concern that are dimension changes associated with the melting and solidification process of the soldering paste. The amount of the latent heat was assessed by adopting the most common SAC (tin-silver-copper) soldering paste (alloy). The study offers the comparison of latent heat with the lead alloy. The sophisticated specimen had to be designed in order to observe the studied effect using thermomechanical analysis (TMA). Results obtained by TMA measurements were compared to simulations. DSC analysis served as a source of input parameters for modeling the studied system via the finite element method (FEM).

2. Experimental

A study of latent heat release was conducted on small square-shaped boards with a size of 9 × 9 mm. The board comprised blind via located in the center. All boards were prepared using a four-layer substrate made of conventional FR4 laminate (JIANGSU RODA

ELECTRON MATERIAL, Rudong, China). The testing board is portrayed in Fig. 1. The diameter of the plated holes was 1.8 mm and its surface was covered by ENIG (Electroless Nickel Immersion Gold) protection. This layout allowed for placing the measuring probe at any distance to solder alloy.

Preparation of specimens for TMA testing was as follows: Solder used for evaluation was obtained by reflowing pieces of solder paste SAC305 (Sn–3%Ag–0.5%Cu) at a non-wetting surface. Arisen balls were weighted to achieve the required value. Then the balls were put into blind holes and the flux was added to support the wetting. Boards with blind via containing the solder balls were reflowed in a three-zone hot air convection oven Mistral 260 (Spidé, Harderwijk, The Netherlands). The reflow profile is depicted in Fig. 2. The reason for using only one profile adjusted for all samples was to ensure the same thermal history.

Dimension change as a function of temperature was measured using a device for thermomechanical analysis TMA Q400 (TA Instruments, New Castle, USA). Samples were heated to 250 °C at a rate of 3 °C/min. The same rate was utilized for cooling back to ambient temperature. A nitrogen atmosphere was maintained in the heating chamber.

The amount of latent heat was derived from the heat flow measured by DSC. DSC analysis was performed at an equipment DSC 131 (SETARAM, Caluire France). Thermal parameters and inert gas were identical as for TMA measurements. Three different masses of solder were used to verify the independence of the amount of latent heat on solder mass. Additionally, in the DSC analysis of lead alloy, Sn63Pb37 was included.

3. Numerical modeling

We perform a simulation of heat transfer and thermal expansion in our device shown in Fig. 3 utilizing FEM as implemented in COMSOL Multiphysics® (COMSOL AB, Stockholm, Sweden). The software solves the heat equation, the equation of motion, and Hooke's law numerically using an automatically generated triangular mesh with density adjusted to the size of individual domains of the device, as shown in Fig. 3. The smaller domains require a denser mesh. Prior to generating the numerical results presented in this manuscript, we performed a convergence study when we tracked the dependence of our results on the mesh density (number of elements). We focused on the dimensions change at solidification shown in Fig. 10. We established that it changes by less than 0.1% at a given temperature when the number of mesh elements is increased above 3000. Therefore, we obtained our numerical results presented here using an automatically generated triangular mesh with 4870 elements in total.

We neglect heat convection and thermal radiation due to the small size of the gas domain and the small variation of temperature within the whole simulation region. The key heat transfer mechanism is the conduction described by the time-dependent heat equation with a source term q_{ext} which is the energy added to the system per unit volume and time:

$$\rho c_p \frac{\partial T}{\partial t} - k\left(\frac{\partial^2 T}{\partial x^2} + \frac{\partial^2 T}{\partial y^2} + \frac{\partial^2 T}{\partial z^2}\right) = q_{ext}(t) \tag{1}$$

ρ is mass density, c_p is heat capacity at constant pressure, k is thermal conductivity, and T is three-dimensional temperature field that we solve for. We focus only on the cooling of the device in an interval from 250 °C to 200 °C, when the latent heat of solidification, $q_{ext}(t)$, is released in the solder. This heat is then dissipated into the surrounding FR4 domain. The effective enthalpy change in a process that involves a solidification is often described by a two-phase model [21,22]:

$$H(T_{hot}) - H(T_{ref}) = \left(\xi(T_{hot}) - \xi(T_{ref})\right)Q_{LH} + \int_{T_{ref}}^{T_{hot}} \left(\xi(T)c_p^{liq} + (1-\xi(T))c_p^{sol}\right)dT \tag{2}$$

where $\xi(T)$ is a smooth transition function from 0 at T_{ref} to 1 at T_{hot}. In our simulation we use $T_{ref} = 200\ ^\circ C$ which is approximately 12 °C below the solidification of the solder (and well above the glass transition of the FR4 board), and $T_{hot} = 250\ ^\circ C$. Our primary goal is to simulate the effect of the latent heat, Q_{LH}, on the thickness of FR4 layer in the vicinity of the first order phase transition. Therefore, we can assume a constant heat capacity $c_p^{liq} = c_p^{sol} \equiv c_p$ and a step-like transition function $\xi(T)$. The enthalpy expression then simplifies to:

$$H(T_{hot}) - H(T_{ref}) = Q_{LH} + c_p\left(T_{hot} - T_{ref}\right) \tag{3}$$

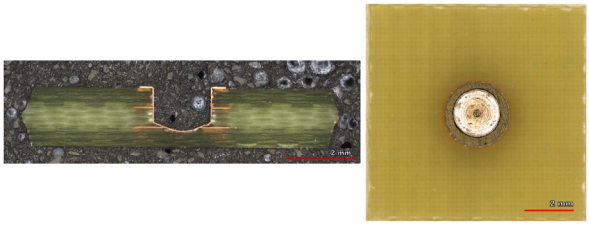

(a) (b)

Fig. 1. Testing board design: (a) cross-section view; (b) top view.

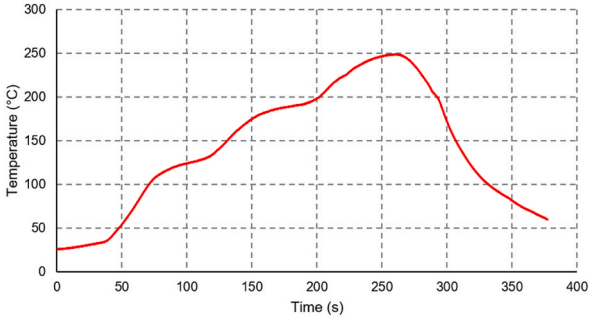

Fig. 2. Temperature profile in hot air convection oven (used for all samples).

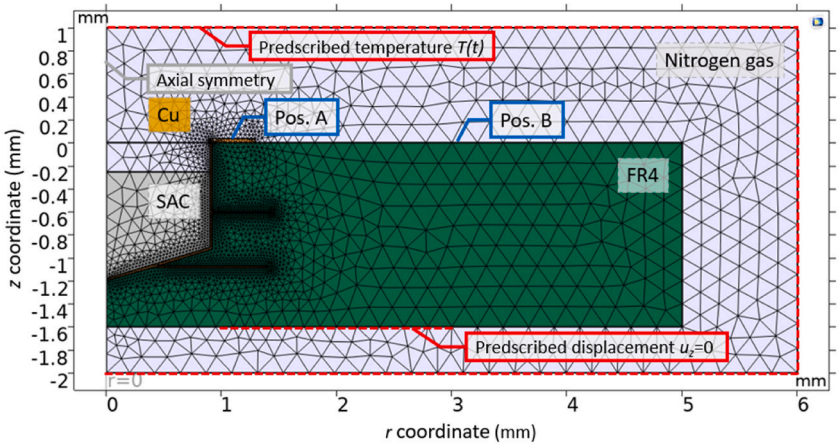

Fig. 3. The cross-section of the device with axial symmetry. Materials and boundary conditions are indicated by colors and red dashed lines, respectively. The triangular mesh with variable density. (For interpretation of the references to color in this figure legend, the reader is referred to the Web version of this article.)

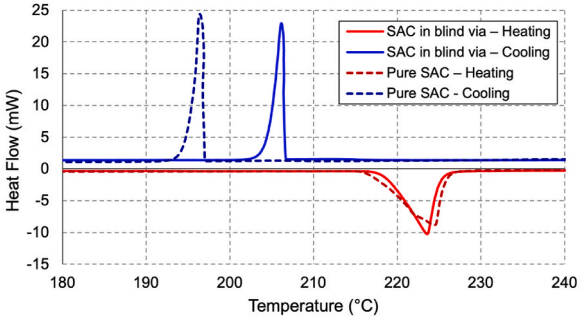

Fig. 4. DSC diagram corresponding to pure SAC alloy and via filled with SAC.

This description of the abrupt (first order) phase transition to solid allows us to model numerically the experimentally observed sudden increase in temperature and consequently a temporary increase of the FR4 thickness at the phase transition.

The latent heat of solidification, Q_{LH}, in our model is related to the external heat source density, $q_{ext}(t)$, of the heat transfer equation (1):

$$Q_{LH} = \frac{1}{\rho}\int q_{ext}(t)dt = \frac{q_{hs}}{\rho}\int \varphi(t)dt \tag{4}$$

We set $Q_{LH} = 62.6$ J/g which is the value measured by DSC (and listed in Table 1 for 14 mg of solder), $\rho = 7.36$ g/cm^3 is the mass density of the solder, and $q_{hs} = 7.68$ MW/m^3 is the corresponding power density which is a direct input of the Comsol model. Function $\varphi(t)$ describes the time-dependence of the heat source as shown in the inset of Fig. 8 – the latent heat is released in a half-minute interval centered at $t = 65.5$ min according to the experimental observation. The amount of solder is set to 14 mg according to the

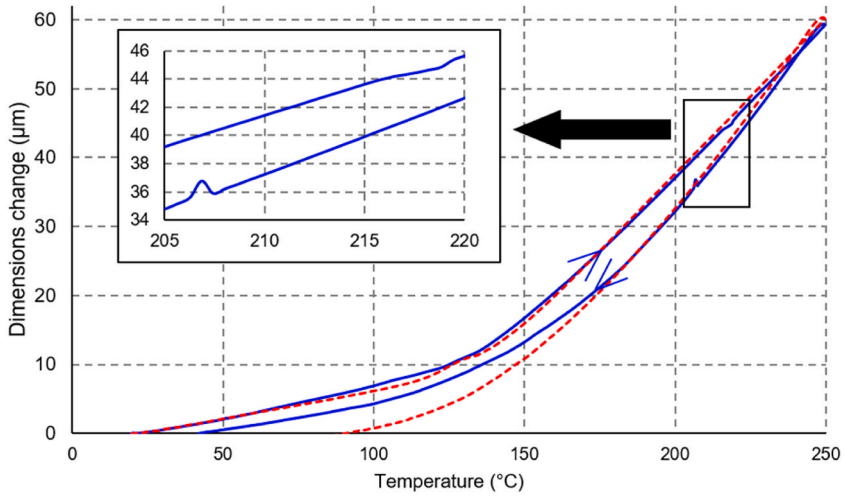

Fig. 5. TMA diagram – expansion probe covering the whole via.

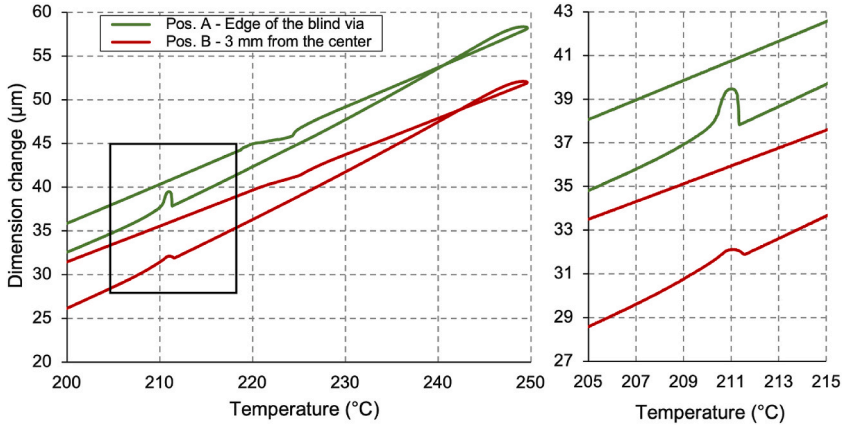

Fig. 6. Effect of latent heat in various distances from the source.

experiment so the total heat released by the solder is 0.875 J.

The temperature variation in our model is coupled to the structural mechanics of the FR4 board via a thermal strain linearly dependent on temperature:

$$\varepsilon_{thermal} = \alpha(T)\left(T - T_{ref}\right) \tag{5}$$

Where $\alpha(T)$ is the linear coefficient of thermal expansion. Again, in our limited temperature range (glass transition is not included), we neglect its dependence on temperature.

The thermal strain then enters our equation of motion, $\nabla \cdot \boldsymbol{\sigma} = \boldsymbol{F}$, describing the structural mechanics of the solid domains of our device. We use the approximation of linear elastic material (except the gas domain) with Hooke's law in the form:

$$\boldsymbol{\sigma} = \boldsymbol{\sigma}_{ext} + \boldsymbol{C} : \boldsymbol{\varepsilon}_{elastic} = \boldsymbol{\sigma}_{ext} + \boldsymbol{C} : (\boldsymbol{\varepsilon} - \boldsymbol{\varepsilon}_{thermal}) \tag{6}$$

where $\boldsymbol{\sigma}$ is the 3x3 stress tensor, $\boldsymbol{\varepsilon}$ is the 3x3 strain tensor $\varepsilon_{ij} = (\nabla_i u_j + \nabla_j u_i)/2$, where u_i is a displacement, and $\boldsymbol{C}$ is the fourth order elasticity tensor which can be parametrized in terms of Young's modulus and Poisson's ratio. We assume isotropic elastic materials. Parameters of materials involved in simulations are listed in Table 1. The values are drawn from cited literature or material datasheet in the case of FR4 laminate. The solder is not solid for most of the temperatures studied, so we use unrealistically low values of Young's modulus and Poisson's ratio as listed in Table 1. A better approximation would be to have temperature-dependent values but the comparison with measured results shows that our simple approximation has sufficient predictive power.

In order to solve the partial differential equations above, we have to provide a set of boundary conditions. These are shown in Fig. 3 as dashed red lines together with the dimensions of our system. We use a model with axial symmetry for the purpose of saving computational resources. The outer boundary of the gas domain is set to a temperature that is swept according to the experimental

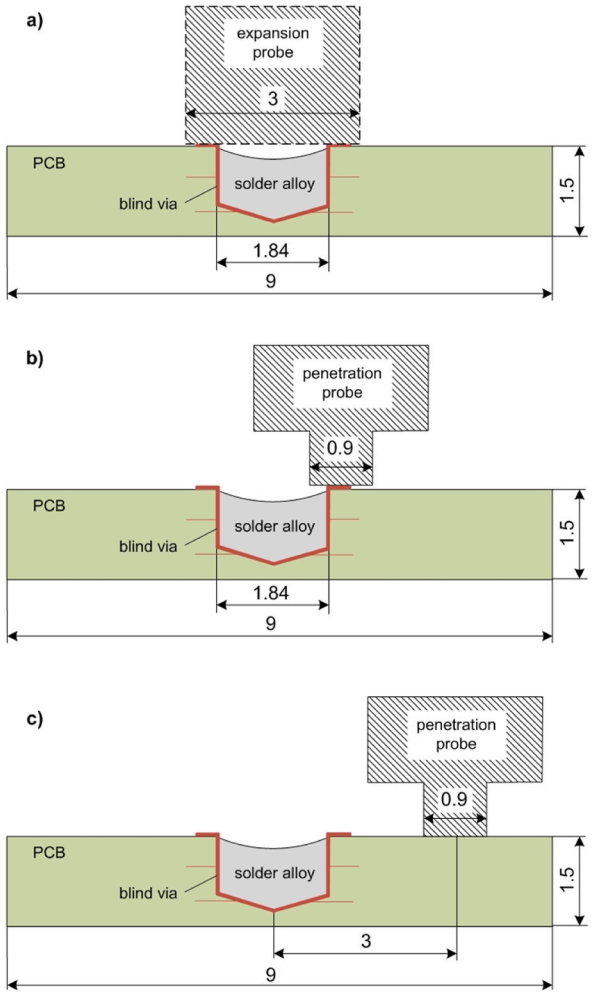

Fig. 7. Illustration of probes placements during TMA: a) probe over the blind via; b) probe on the edge of the blind via – corresponds to Pos. A in Figs. 3 and 10; c) probe on PCB substrate – corresponds to Pos. B in Figs. 3 and 10.

cooling process from 250 to 200 °C. The boundary of the structural mechanics domains is set to free displacement except for a section of the bottom surface which is set to $u_z = 0$ with the aim of describing contact with the surface of a glass stage (which is not part of the model). The radial expansion occurs with respect to the center (r = 0). Fig. 3 also encodes the different materials via the colors. Latent heat is released in the SAC domain. Positions A and B indicate the locations where the dimension change is measured.

4. Results and discussion

4.1. Evaluation through DSC and TMA

Before investigating the impact of latent heat on dimensional conditions, accurate thermal properties of melting and solidification had to be analyzed. Therefore, DSC diagrams were measured and the latent heat per mass, Q_{LH}, was determined using DSC software for analyzing the data. The resulting values (available in Table 2) were obtained by integrating the area enclosed under the peak of the heat curve. This statement can be mathematically written as

$$Q_{LH} = \frac{1}{\beta}\int_{T_{end}}^{T_{onset}} \left(\frac{dQ(T)}{dt} - f(T)\right) dT \tag{7}$$

where β is sampling velocity (K/s), $\frac{dQ(T)}{dt}$ is released heat (W) and $f(T)$ stands for the approximated baseline connecting the measured curve before and after phase transition. The function in our analyses was represented by a straight line (linear function). Three different alloy's weights were analyzed to ascertain the independency on the measured bulk. The correctness of the latent heat results was verified by comparing them with those summarised in the work of Morando et al. [21] where 66.9 J/g is presented for SAC alloy. Latent heat figures for lead solder alloy are approximately 50% lower than those for SAC due to the lower content of tin. Therefore, the

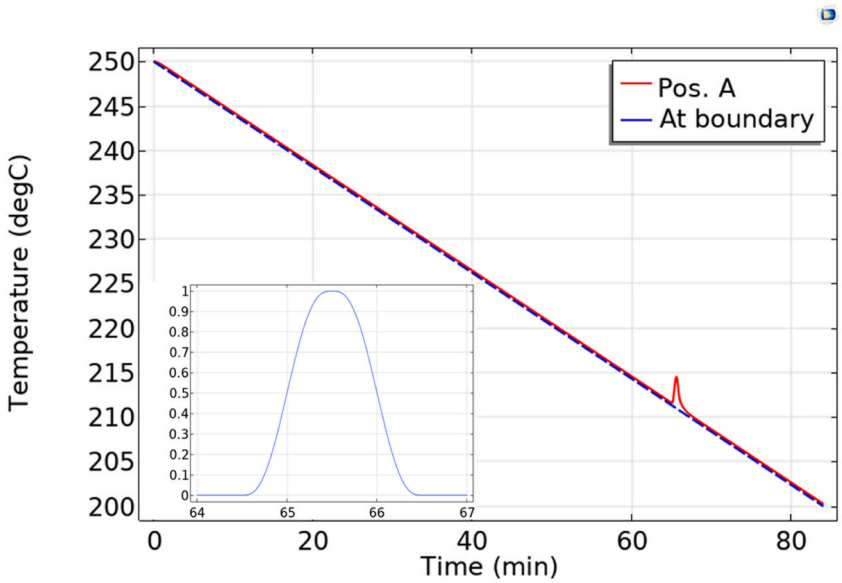

Fig. 8. The temperature at position A and at the simulation region boundary (driven linear decrease) during the cooling process which lasts 84 min.

importance of assessing the latent heat impact has become more desirable since the elimination of lead alloys.

Moreover, we performed a DSC analysis of the blind vias filled by reflowed solder alloy. For this purpose, vias were removed from the testing boards to contain only negligible remains of the laminate that may influence the DSC measurements. Diffusion of golden and nickel particles from the surface finish takes place during soldering, as Yoon et al. [27] reviewed in their study, and notably changes the transition temperatures. Fig. 4 contains the resulting DSC curves for pure SAC alloy (14 mg) and SAC included in the blind vias. The most important finding arising from the measurement is the detection of reduced undercooling, i.e., a shorter interval between the melting and solidification for alloy contaminated by gold and nickel. This fact is attributed to the formation of nucleation centers that are responsible for higher solidification temperature, as it was explained in the study done by Rudajevová and Dušek [28]. Another distinction in Fig. 4 is visible on the heating courses. During heating, the supplied heat is consumed for the melting. It results in the eliminated increase of the heat flow that relates to the smaller negative peak and the spread of the peak over a wider temperature interval. Decalescence relates to this observation which means delaying the temperature rise of the sample. On the contrary, a hint of recalescence can be seen on the blue dashed curve as the heat flow increase tends to move to higher temperature values than the peak begins.

The curve depicted in Fig. 5 was attained by using the expansion probe, which was placed on the via (see Fig. 7a). The red curve corresponds to an empty blind barrel and the blue one was measured on a barrel filled with 14 mg of SAC alloy. This curve has a typical shape for laminate, i.e., a knee where Tg is defined and CTE undergoing enormous change is obvious. Particularly, there is a noticeable plateau in dimension change during heating as a consequence of latent heat of fusion. Furthermore, a peak developed when the board was cooling down and the alloy turned into a solid state. It is a consequence of the latent heat of solidification. According to a location in temperature axis, it can be seen that both of these phenomena nearly correspond with the peaks in Fig. 4.

Further measurements on thermomechanical analyzer employed the probe with a thin spike (0.9 mm) that allows focusing on a given location with higher accuracy. Using this probe, two curves were obtained. Fig. 6 shows the relevant parts of them. The relation between the curves and probe placement is portrayed in Fig. 7. Position A correlates with the arrangement shown in Fig. 7b and position B with that in Fig. 7c. The height of the peak during solidification on the edge of the barrel is 1.6 μm and is slightly higher than the in the previous case shown in Fig. 5 and the arrangement depicted in Fig. 7a. As to the time duration of the observed peak, the growth and decrease of temperature take approximately 30 s. When the probe moved to a distance of 3 mm away from the barrel center, the peak was barely registered (approx. 0.3 μm high). Nevertheless, it proves the heat transfer through the substrate and the possibility of affecting more distant surroundings. Considering more complex PCB where the components are very close to each other, the resulting impact on the substrate expansion can be multiplied. Our measurement with the probe located 6 mm from the blind via center showed no signs of impact on the dimensions of the board.

Finally, we note that the transition temperatures vary slightly as indicated by positions of peaks in the measured DSC and TMA curves above. This may be caused by small deviations of the internal structure of the solder in individual samples. Despite repeating the same study procedure parameters, the melted solder contains elements influencing the formation of nucleation centers [29]. Hence, the undercooling is impacted and the corresponding solidification temperature may vary.

4.2. FEM simulation

The first result of our simulation is the decrease of temperature over time, as shown in Fig. 8. The temperature at the boundary of the simulation region describes the linear cooling imposed by the experimental setup (TMA). The temperature at position A follows the

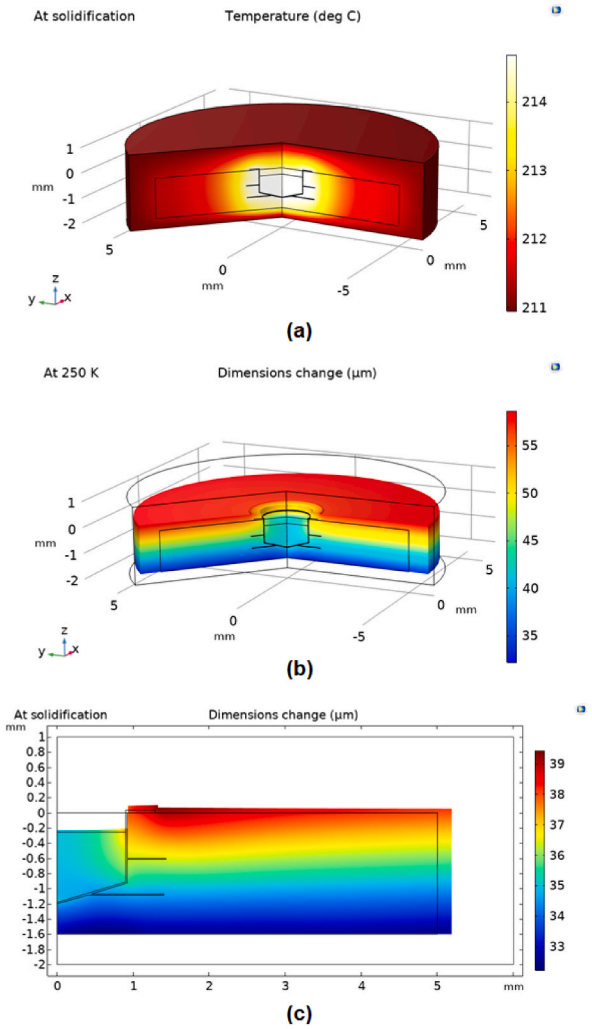

Fig. 9. Simulation results: (a) the temperature on the surface of the simulation region; (b) the dimension change (displacement u_z) in the vertical direction; (c) the dimension change in the cross-section of the sample.

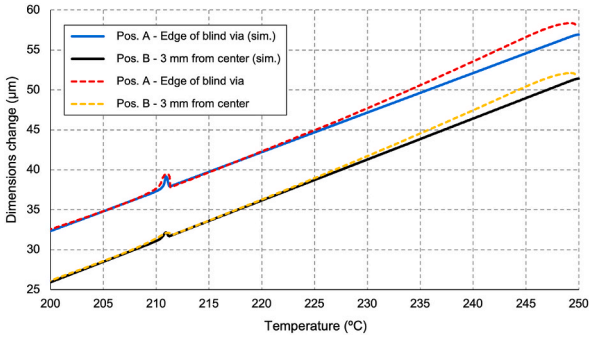

Fig. 10. The dimension change (displacement u_z) at positions A and B as a function of temperature. Solid and dashed lines correspond to measured and simulated data, respectively.

externally driven cooling very closely which demonstrates good thermal coupling between the device and its surroundings. (This is due to the slow cooling rate and small volume of the gas domain with low thermal conductivity.) The peak in temperature at position A at $t \approx 65$ minutes is the only exception which is caused by the released latent heat of solidification. The inset of Fig. 8 shows the function $\varphi(t)$ which describes the time dependence of the heat source in relation to eq. (4).

Table 1
Material parameters used as input of model.

Parameter	SAC305 [23]	FR4			Cu [24]
Mass density [g/cm^3]	7.36	1.9			8.96
Heat capacity [J/kg/K]	234	1400 [25]			383
Thermal conductivity [W/K/m]	59	0.3 $\perp$	1.01 $\parallel$	[26]	386
Thermal expansion coeff. [ppm/K]	22	317			16.5
Young's modulus [GPa]	0.01 (40)	22			124
Poisson's ratio	0.04 (0.3)	0.15			0.34

Table 2
Amount of latent heat for both phase changes for SAC and SnPb solder alloy in J/g.

Solder alloy	SAC305		Sn63Pb37	
Weight (mg)	Heating	Cooling	Heating	Cooling
7	64,8	62,4	44,1	39,7
14	65,1	62,6	42,6	37,9
21	65,8	62,9	42,6	38,9

Fig. 9a shows the overall temperature distribution at solidification when the latent heat causes local temperature elevation around the barrel. This is visible in the cross-section of the simulation region with axial symmetry.

Fig. 9b shows the dimension change (displacement u_z) in the vertical direction induced by thermal expansion from room temperature to 250 °*C*. The figure includes the deformation of the whole device with respect to the original dimensions (black lines) multiplied by 10 to make the deformation easier to see. Note that the barrel deforms less than FR4 due to the lower thermal expansion coefficient of the solder and copper. We set the deformation at T_{ref} to the experimental values as it is hard to model the change of dimensions of the FR4 slab during its glass transition – inhomogeneities of material properties are likely.

Fig. 9c shows the dimension change in a cross-section (without the axial symmetry applied) at solidification. We note that the vertical thermal expansion is larger closer to the barrel than compared to the edge.

Fig. 10 shows the main result of our study which is the comparison of the simulated and measured dimension change (displacement u_z) at positions A and B as a function of temperature. We have already mentioned that modeling the non-linear expansion of FR4 during the glass transition using our model (assuming a homogenous FR4 layer) would be prohibitively complicated so we set the displacement at $T_{ref} = 200$ °C to the experimental value for each position. Furthermore, we use the linear thermal expansion coefficient of FR4 which co-determines the slope of the curves in Fig. 10 as a fitting parameter. (It means that CTE is considered to be a temperature-independent parameter above the glass transition.) We obtain $\alpha = 317$ ppm/K, which is in the range 300–320 ppm/K expected based on experimental observation.

Adopting the linear thermal expansion implies slight inconsistency of modeled dimension change (solid line) and measured one (dashed line) in Fig. 10 noticeable above 230 °C. The measured substrate dimension change shows small deviations from a linear dependence on temperature. However, it is common to approximate it by a linear function with two different values of CTE under and above the glass transition [30]. Another factor influencing the difference between the compared curves in Fig. 10 is that the TMA analysis was conducted to 250 °C. The response of the substrate in the transition from heating to cooling may play a certain role in the non-linear behavior at the beginning of the cooling phase. Nevertheless, the studied phenomenon takes place at a lower temperature than the slight mismatch occurs. Therefore, it does not affect the model accuracy established to describe the latent heat release at approximately 211 °C.

The amount of solder, the latent heat, and the initial dimensions of the board and barrel are set to the experimental values. This approach allows us to focus on the effect of the latent heat of solidification on the dimension change. For this choice of input parameters, we obtain the dimension change as a function of temperature in excellent quantitative agreement with the experiment. To quantify this agreement, we compare the size of the measured and simulated local maximum of the dimensions change at 211 °C, as shown in Fig. 10. Experimentally, the peak value of 39.47 μm occurs at 211 °C and the dip of 37.83 μm occurs at 211.35 °C. The corresponding simulated values are 39.17 and 37.92 μm, respectively. The relative size of the local peak is 1.64 and 1.25 μm in the experiment and the simulation, respectively. In the case of this value, we note that the size of the peak related to recalescence is strongly dependent on the duration of the solidification (how fast is the latent heat released) and on the thermal conductivity of FR4 substrate (how fast is the heat dissipated into the environment). It is beyond the scope of this paper to further improve the accuracy of the measurement of these two parameters. Their limited accuracy can explain the difference between the size of the simulated and measured peak at solidification.

Based on this comparison, we can conclude that our FEM model is capable of describing the thermal expansion of FR4 board caused by the latent heat released during cooling in the adjacent barrel filled with solder. We note that this mechanism cannot be described only by a change of heat capacity with temperature.

5. Conclusions

Thermomechanical analysis in conjunction with a specially designed board was used to investigate the influence of latent heat on

substrate expansion. This approach allowed us to demonstrate the direct influence of solder phase change on the vertical dimension of the surrounding substrate material. Measurements proved the impact during both phase changes. The more significant phenomenon in the form of a sharp peak occurs when the solder alloy solidifies. The substrate material is affected at a significant distance from the via, as confirmed by our measurement of the sudden rise of vertical dimension as far as 3 mm from the alloy (more than the typical distance between neighboring joints on a PCB). If more heat sources (solder joints) were concentrated in a small area, they would induce a substrate expansion with the potential threat of creating unreliable solder joints or damage of nearby parts of the PCB. Accurate latent heat magnitudes obtained by DSC confirmed that the observed phenomenon is more notable in lead-free soldering.

Measured values of dimensions change were compared to our numerical model in Fig. 10. The model is focused on the cooling part of the cycle. Excellent agreement of simulated and measured dimension changes was observed. A comparison of the size of the measured and simulated local maximum of the dimensions change at 211 °C verifies the model agreement with experimental observations. In the experiment, the peak reaches the height of 39.47 μm at 211 °C and the dip of 37.83 μm occurs at 211.35 °C. The model provides values of 39.17 and 37.92 μm after simulation. We also compared the maximum height of the local peak. Comparing this value, a small discrepancy between the experiment and the simulation appears. The reason was discussed and explained. Despite this fact, the overall comparison confirms the predictive power of our FEM based model and the importance of managing the dissipation of latent heat in reflow soldering of boards with a high density of joints.

Finally, the numerical model refined in this case study can predict the behavior of PCBs and solder joints with similar spatial and material composition to that studied here. Therefore, it can be used in the future to model PCBs with an accumulation of solder joints in a small area and indicate situations with a high risk of damage to the joints or the board. Such a model-based approach is faster and cheaper than the preparation of a range of samples and conducting TMA for each case.

Declaration of competing interest

The authors declare that they have no known competing financial interests or personal relationships that could have appeared to influence the work reported in this paper.

Acknowledgment

This work was supported by the Grant Agency of the Czech Technical University in Prague, grant No. SGS21/159/OHK3/3T/13.

References

[1] T.-N. Tsai, Thermal parameters optimization of a reflow soldering profile in printed circuit board assembly: a comparative study, Appl. Soft Comput. 12 (8) (Aug. 2012) 2601–2613, https://doi.org/10.1016/j.asoc.2012.03.066.
[2] A. Rudajevová, K. Dušek, Influence of manufacturing mechanical and thermal histories on dimensional stabilities of FR4 laminate and FR4/Cu-plated holes, Materials 11 (11) (Oct. 2018) 2114, https://doi.org/10.3390/ma11112114.
[3] R. Sanapala, B. Sood, D. Das, M. Pecht, Effect of lead-free soldering on key material properties of FR-4 printed circuit board laminates, IEEE Trans. Electron. Packag. Manuf. 32 (4) (Oct. 2009) 272–280, https://doi.org/10.1109/TEPM.2009.2029566.
[4] A. Rudajevova, K. Dušek, Residual strain in PCBs with Cu-plated holes, J. Electron. Mater. 46 (12) (Dec. 2017) 6984–6991, https://doi.org/10.1007/s11664-017-5714-3.
[5] B. Birch, Reliability testing for microvias in printed wire boards, Circ. World 35 (4) (Nov. 2009) 3–17, https://doi.org/10.1108/03056120911002361.
[6] S. Chung, J.B. Kwak, Realistic warpage evaluation of printed board assembly during reflow process, Solder. Surf. Mt. Technol. 27 (4) (Sep. 2015) 137–145, https://doi.org/10.1108/SSMT-12-2014-0023.
[7] Y. Ko, H. Park, G. Park, S. Cho, A study on the reliability of micro-vias in printed circuit boards during thermal cycling, Adv. Sci. Lett. 19 (12) (Dec. 2013) 3683–3687, https://doi.org/10.1166/asl.2013.5193.
[8] Y. Ning, M.H. Azarian, M. Pecht, Development of a microvia fatigue life model using a response surface method, IEEE Trans. Device Mater. Reliab. 19 (1) (Mar. 2019) 176–188, https://doi.org/10.1109/TDMR.2019.2898179.
[9] K.M. Reutzel, Utilizing thermal fatigue testing to differentiate the performance of epoxy materials at various glass transition temperature levels, Circ. World 26 (1) (Jan. 2000) 16–18, https://doi.org/10.1108/03056120010302151.
[10] B. Illés, Distribution of the heat transfer coefficient in convection reflow oven, Appl. Therm. Eng. 30 (13) (Sep. 2010) 1523–1530, https://doi.org/10.1016/j.applthermaleng.2010.02.016.
[11] A. Géczy, Investigating heat transfer coefficient differences on printed circuit boards during vapour phase reflow soldering, Int. J. Heat Mass Tran. 109 (Jun. 2017) 167–174, https://doi.org/10.1016/j.ijheatmasstransfer.2017.01.091.
[12] Y. Liu, P. Fiacco, N.-C. Lee, Testing and prevention of head-in-pillow, in: 2010 Proceedings 60th Electronic Components and Technology Conference (ECTC), Las Vegas, NV, USA, 2010, pp. 451–455, https://doi.org/10.1109/ECTC.2010.5490931.
[13] D. Bušek, K. Dušek, M. Plaček, J. Urbánek, J. Horník, J. Holec, Determination of BGA solder joint detachment cause - warpage effect, in: 2015 38th International Spring Seminar on Electronics Technology (ISSE), May 2015, pp. 306–309, https://doi.org/10.1109/ISSE.2015.7248011.
[14] H. Wohlrabe, K. Meier, O. Albrecht, Influences of SMD package and substrate warpage on quality and reliability –measurement, effects and counteractions, in: 2018 7th Electronic System-Integration Technology Conference (ESTC), Dresden, Sep. 2018, pp. 1–6, https://doi.org/10.1109/ESTC.2018.8546438.
[15] A. Pietrikova, T. Lenger, O. Fricova, L. Popovic, L. Livovsky, Properties of glass/epoxy sandwich structure for electronic boards, MI 37 (3) (Mar. 2020) 139–146, https://doi.org/10.1108/MI-12-2019-0084.
[16] K.-W. Moon, W.J. Boettinger, U.R. Kattner, F.S. Biancaniello, C.A. Handwerker, Experimental and thermodynamic assessment of Sn-Ag-Cu solder alloys, J. Electron. Mater. 29 (10) (Oct. 2000) 1122–1136, https://doi.org/10.1007/s11664-000-0003-x.
[17] K. Dušek, A. Rudajevová, M. Plaček, Influence of latent heat released from solder joints on the reflow temperature profile, J. Mater. Sci. Mater. Electron. 27 (1) (Jan. 2016) 543–549, https://doi.org/10.1007/s10854-015-3787-4.
[18] C. Morando, O. Fornaro, O. Garbellini, H. Palacio, Fluidity of Sn-based eutectic solder alloys, J. Mater. Sci. Mater. Electron. 26 (12) (Dec. 2015) 9478–9483, https://doi.org/10.1007/s10854-015-3415-3.
[19] K. Dusek, V. Zahradnik, P. Vesely, D. Busek, M. Placek, Released of latent heat from solder joints to surrounding during solidification of solder alloy - experimental study, in: 2019 42nd International Spring Seminar on Electronics Technology (ISSE), Wroclaw, Poland, May 2019, pp. 1–4, https://doi.org/10.1109/ISSE.2019.8810199.
[20] K. Dušek, A. Rudajevová, Influence of latent heat released from solder joints II: PCB deformation during reflow and pad cratering defects, J. Mater. Sci. Mater. Electron. 28 (1) (Jan. 2017) 1070–1077, https://doi.org/10.1007/s10854-016-5630-y.

[21] C. Morando, O. Fornaro, O. Garbellini, H. Palacio, Thermal properties of Sn-based solder alloys, J. Mater. Sci. Mater. Electron. 25 (8) (Aug. 2014) 3440–3447, https://doi.org/10.1007/s10854-014-2036-6.
[22] T. Barz, J. Emhofer, K. Marx, G. Zsembinszki, L.F. Cabeza, Phenomenological modelling of phase transitions with hysteresis in solid/liquid PCM, J. Build. Perform. Simul. 12 (6) (Nov. 2019) 770–788, https://doi.org/10.1080/19401493.2019.1657953.
[23] K. Shinohara, Q. Yu, Fatigue life evaluation accuracy of power devices using finite element method, Int. J. Fatig. 33 (9) (Sep. 2011) 1221–1234, https://doi.org/10.1016/j.ijfatigue.2011.03.009.
[24] S. Yin, X. Wang, W. Li, B. Xu, Numerical investigation on effects of interactions between particles on coating formation in cold spraying, J. Therm. Spray Technol. 18 (4) (Dec. 2009) 686–693, https://doi.org/10.1007/s11666-009-9390-6.
[25] F. Sarvar, P.P. Conway, Effective modeling of the reflow soldering process: basis, construction, and operation of a process model, IEEE Trans. Compon. Packag. Manuf. Technol. C 21 (2) (Apr. 1998) 126–133, https://doi.org/10.1109/3476.681389.
[26] F. Sarvar, N.J. Poole, P.A. Witting, PCB glass-fibre laminates: thermal conductivity measurements and their effect on simulation, JEM 19 (12) (Dec. 1990) 1345–1350, https://doi.org/10.1007/BF02662823.
[27] J.-W. Yoon, W.-C. Moon, S.-B. Jung, Interfacial reaction of ENIG/Sn-Ag-Cu/ENIG sandwich solder joint during isothermal aging, Microelectron. Eng. 83 (11–12) (Nov. 2006) 2329–2334, https://doi.org/10.1016/j.mee.2006.10.027.
[28] A. Rudajevová, K. Dušek, Study of undercooling and recalescence during solidification of Sn62.5Pb36.5Ag1 and Sn96.5Ag3Cu0.5 solders in real electronic joints, J. Electron. Mater. 43 (7) (Jul. 2014) 2479–2486, https://doi.org/10.1007/s11664-014-3121-6.
[29] G. Parks, A. Faucett, C. Fox, J. Smith, E. Cotts, The nucleation of Sn in undercooled melts: the effect of metal impurities, J. Occup. Med. 66 (11) (Nov. 2014) 2311–2319, https://doi.org/10.1007/s11837-014-1161-2.
[30] Y.K. Kim, Viscoelastic effect of FR-4 material on packaging stress development, IEEE Trans. Adv. Packag. 30 (3) (Aug. 2007) 411–420, https://doi.org/10.1109/TADVP.2007.901294.